以磁性碳纳米球为载体的锂离子印迹吸附剂用于锂离子的选择性回收

梁 琦[1]，张二辉[2]，闫 光[1]，杨永珍[1]，刘伟峰[1,3]，刘旭光[1,3]

（1. 太原理工大学 新材料界面科学与工程教育部重点实验室，山西 太原 030024；
2. 太原理工大学 化学化工学院，山西 太原 030024；
3. 太原理工大学 新型碳材料研究院，山西 晋中 030600）

摘 要： 以磁性碳纳米球（Fe_3O_4@C）为载体，2-羟甲基-12-冠醚-4为吸附单元，采用表面离子印迹技术设计并制备了对Li^+具有选择性吸附的磁性碳基锂离子印迹材料（Li^+-IIP-Fe_3O_4@C）。首先，采用γ-甲基丙烯酰氧基丙基三甲氧基硅烷对Fe_3O_4@C进行改性，得到硅烷化Si-Fe_3O_4@C。接着用甲基丙烯酸（MAA）对Si-Fe_3O_4@C进行功能化，得到形貌规整且具有较高MAA接枝度的PMAA-Fe_3O_4@C。然后，借助催化剂对甲苯磺酸将2-羟甲基-12-冠醚-4接枝到PMAA-Fe_3O_4@C的表面，进一步在二甲基丙烯酸乙二醇酯的交联聚合下得到Li^+-IIP-Fe_3O_4@C。动力学吸附和等温吸附结果表明，Li^+的吸附符合准二级动力学模型和Langmuir等温模型。Li^+-IIP-Fe_3O_4@C在25 °C下对Li^+的最大吸附容量达到22.26 mg g^{-1}。Li^+相对于Na^+，K^+和Mg^{2+}的选择因子分别为8.06、5.72和2.75。经6次吸附-解吸循环，Li^+-IIP-Fe_3O_4@C的吸附容量仅降低了8.8%，表现出优异的再生性能。

关键词： 吸附；印迹吸附剂；锂离子；磁性；碳纳米球

中图分类号： TB33 **文献标识码：** A

基金项目：科技部国家重点研发计划（2017YFB0603104）；国家自然科学基金（U1607120，U1610255，51603142）；山西省重点研发计划国际合作项目（201903D421077）.

通讯作者：杨永珍，博士，教授. E-mail：yyztyut@126.com
刘伟峰，博士，副教授. E-mail：lwf061586@yeah.net
作者简介：梁 琦，硕士研究生. E-mail：2498435356@qq.com

A lithium ion-imprinted adsorbent using magnetic carbon nanospheres as a support for the selective recovery of lithium ions

LIANG Qi[1], ZHANG Er-hui[2], YAN Guang[1], YANG Yong-zhen[1], LIU Wei-feng[1,3], LIU Xu-guang[1,3]

(1. *Taiyuan University of Technology, Key Laboratory of Interface Science and Engineering in Advanced Materials, Ministry of Education, Taiyuan* 030024, *China*;
2. *Taiyuan University of Technology, College of Chemistry and Chemical Engineering, Taiyuan* 030024, *China*;
3. *Taiyuan University of Technology, Institute of New Carbon Materials, Jinzhong* 030600, *China*)

Abstract: A magnetic carbon-based lithium ion – imprinted material (Li^+-IIP-Fe_3O_4@C) with a high Li^+ adsorption selectivity was designed and prepared by a surface ion imprinting method, using magnetic carbon nanospheres (Fe_3O_4@C) as the carrier and 2-hydroxymethyl-12-crown-4 as the adsorption unit. First, Fe_3O_4@C was silanized by γ-methacryloxypropyltrimethoxysilane to obtain Si-Fe_3O_4@C which was then functionalized with methacrylic acid (MAA), followed by polymerization to obtain PMAA-Fe_3O_4@C with a regular morphology and a high degree of MAA grafting. Finally, 2-hydroxymethyl-12-crown-4 was grafted onto the surface of PMAA-Fe_3O_4@C in the presence of $LiClO_4$ under catalysis by p-toluenesulfonic acid. This was cross-linked by ethylene glycol dimethacrylate and eluted by a HNO_3 solution to obtain Li^+-IIP-Fe_3O_4@C. The kinetic adsorption and isothermal adsorption results for this material show that the adsorption of Li^+ conforms to a pseudo-second-order kinetic model and has Langmuir isotherms. The maximum adsorption capacity of Li^+-IIP-Fe_3O_4@C for Li^+ is 22.26 mg/g at 25 °C. The selection factors of Li^+ against Na^+, K^+ and Mg^{2+} are 8.06, 5.72, and 2.75, respectively. The Li^+ adsorption capacity of Li^+-IIP-Fe_3O_4@C decreases by only 8.8% after six adsorption-desorption cycles, demonstrating an excellent regeneration capability and making it very useful for lithium recovery.

Key words: Adsorption; Imprinted absorbent; Lithium ion; Magnetic; Carbon nanospheres

Received date: 2020-03-05; *Revised date*: 2020-04-20

Foundation item: National Key Research and Development Program of China (2017YFB0603104), National Natural Science Foundation of China (U1607120, U1610255, 51603142), Key R&D Program of Shanxi Province (International Cooperation, 201903D421077).

Corresponding authors: YANG Yong-zhen, Ph. D, Professor. E-mail: yyztyut@126.com
LIU Wei-feng, Ph. D, Professor. E-mail: lwf061586@yeah.net
Author introduction: LIANG Qi, Master student. E-mail: 2498435356@qq.com

1 Introduction

Lithium is considered to be an "energy metal for promoting world progress", owing to its many superior electrochemical and physical properties to other metals[1, 2]. Up to now, all the inventory of explored lithium resources has achieved 5.4 million tons in China, of which the lithium from the salt lake brine accounts for about 61.8%. The large amount of lithium resources in the salt lake brine has opened up a new path for the acquisition of lithium[3, 4]. Therefore, the extraction of lithium from the salt lake brine has caused abroad attention[5].

Now, the methods for extracting lithium from the salt lake brine include adsorption[6-8], solvent extraction[9, 10], precipitation method[11], and so on, among which adsorption is the most adopted one owing to its advantages of simple operation and low energy consumption.

The composition of the salt lake brine is complex, with the existence of Li, Na, K, Mg[12-14], which makes it difficult to solely extract lithium. For highly efficient lithium extraction by adsorption, absorbents are needed to possess high selectivity. As a new type of a selective adsorption technology, surface imprinting[15, 16] is different from the conventional imprinting techniques[17]. It creates memory sites[18] on the surface of a substrate, which improves the selectivity of an absorbent. What's more, the high selectivity of an adsorbent also depends on recognition by an adsorption unit. Crown ether is a novel kind of an annular chelator[19]. Its biggest feature is that its appropriate ring size can be well coordinated with positive ions, especially alkali metal ions. A plurality of C—O dipoles in the molecule can coordinate with different metal ions to form different complex as the size of the ring changes. The inner diameter of 12-crown-4[20] is 0.15 nm, which is similar to the size of Li^+ (0.152 nm)[21]. Therefore, 12-crown-4 is expected to exhibit a good stereoselectivity for lithium ions[22].

Meanwhile, the adsorbent material should have a high regenerability and adsorption capacity to lower the adsorption operation cost. Currently, the adsorbing materials are prepared by using polymers, SiO_2 encapsulated magnetic particles and carbon materials[23, 24] as supports. Cui et al[25] adopted precipitation polymerization to synthesize a lithium ion imprinted polymer, whose adsorption capacity (6.79 mg g^{-1}) was not high enough but without a significant decline after six adsorption and desorption cycles. Luo et al[26] prepared a Li^+ imprinted polymer on the surface of Fe_3O_4@SiO_2 with 2-(allyloxy) methyl-12-crown-4 as a functional monomer, whose adsorption capacity (4.07 mg g^{-1}) was not high but declined only by 7.6% after five cycles due to its perfect magnetic performance. Huang et al[27] chose dibenzo-14-crown-4 as a functional monomer to synthesize a lithium ion imprinted polymer on the surface of multi-walled carbon nanotubes, which showed a low adsorption (9.46 mg g^{-1}) but a high regenerability. After 10 cycles of adsorption-desorption, the adsorption capacity only decreased by 10.3%. From the above-mentioned researchers, it can be concluded that it is of urgent necessity to prepare an absorbent with both a high adsorption capacity and a high regenerability.

Magnetic carbon nanospheres possess good biocompatibility, mechanical stability, and magnetism[28, 29] that is in favor of subsequent separation. Meanwhile, magnetic carbon nanospheres exhibit high surface activity, which is beneficial to stably loading an adsorption unit by modification and grafting[30]. Therefore, magnetic carbon nanospheres can be used as the supporting material for surface imprinting to obtain a lithium ion imprinted absorbent with a high selectivity and lithium ion adsorption capacity. In this work, Fe_3O_4@C prepared by the solvothermal method was modified with KH-570 to prepare Si-Fe_3O_4@C. Further, methacrylic acid (MAA) was used as a functional monomer to modify Si-Fe_3O_4@C surface to obtain PMAA-Fe_3O_4@C. During preparation of PMAA-Fe_3O_4@C, the initiator AIBN dosage was optimized. Later, surface ion imprinting technology was adopted with 2-hydroxymethyl-12-crown-4 as the adsorption unit, Li^+ as the target ion, p-toluenesulfonic acid as the catalyst and ethylene glycol dimethacrylate as the cross-linking agent to create an imprinted layer on the surface of PMAA-Fe_3O_4@C. Li^+-IIP-Fe_3O_4

@C with a high selective adsorption capacity for Li^+ was obtained after eluting Li^+. In this process, the influence of the p-toluenesulfonic acid dosage and reaction temperature on the adsorption capacity of Li^+-IIP-Fe_3O_4@C for Li^+ was investigated. Finally, the selectivity in adsorption and regeneration performance of Li^+-IIP-Fe_3O_4@C towards Li^+ were explored.

2 Experimental

2.1 Materials and reagents

Ferrocene, absolute ethanol, MAA, N,N-dimethylformamide (DMF), p-toluenesulfonic acid and glacial acetic acid were purchased from Tianjin Guangfu Technology Development Co., Ltd. Lithium perchlorate ($LiClO_4$) was purchased from Beijing Innochem Science & Technology Co., Ltd. Acetone, hydrogen peroxide (H_2O_2) and γ-methacryloxypropyltrimethoxysilane (KH-570) were purchased from Tianjin Tianli Chemical Reagent Co., Ltd. Azobisisobutyronitrile (AIBN) was provided by Tianjin Fuchen Chemical Reagent Factory. 2-hydroxymethyl-12-crown-4 and ethyleneglycol dimethacrylate (EGDMA) were obtained from Alfa Aesar Chemical Co., Ltd. Nitric acid was purchased from Luoyang Chemical Reagent Factory.

2.2 Preparation of Li^+-IIP-Fe_3O_4@C

First of all, the magnetic carbon nanospheres (Fe_3O_4@C) with a particle size of ~90 nm and an amorphous carbon layer thickness of ~13 nm, were obtained, and then silanized by KH-570 to obtain silanized magnetic carbon nanospheres (Si-Fe_3O_4@C) according to our previous work[31, 32]. Next, Si-Fe_3O_4@C (0.1 g), acetonitrile (30 mL) and MAA (0.01 mol) were sequentially added to a three-necked flask under ultrasonic dispersion for 10 min. The mixture was heated to 65 °C in a water bath. After 10 min, AIBN was added into the solution to initiate the polymerization of MAA, during which the influence of the AIBN dosage (0.000 2, 0.000 5, and 0.001 mol) on the grafting efficiency of MAA was investigated. Finally, PMAA-Fe_3O_4@C was obtained under the optimized AIBN dosage. The MAA grafting efficiency on the surface of PMAA-Fe_3O_4@C was calculated by the following equation (1):

$$D_g = [(W_{later} - W_{former})/W_{former}] \times 100\% \quad (1)$$

Where D_g represents MAA grafting efficiency. W_{later} and W_{former} are the weight loss of Si-Fe_3O_4@C and PMAA-Fe_3O_4@C, respectively.

On the basis of as-obtained PMAA-Fe_3O_4@C, Li^+-IIP-Fe_3O_4@C was synthesized by the surface ion imprinting technique. $LiClO_4$ (0.5 mmol) and 2-hydroxymethyl 12-crown-4 (0.5 mmol) were put into 20 mL of DMF. The system was stirred at 25 °C for 2 h to achieve self-assembly of the functional monomer and lithium ions. After that, PMAA-Fe_3O_4@C (0.1 g) obtained under the optimized conditions and p-toluenesulfonic acid were added and reacted at a designed temperature for 6 h, during which the influence of the p-toluenesulfonic acid dosage (30, 60, 90, 120 and 150 mg) and reaction temperature (60, 80, 100 and 120 °C) on the immobilization of 2-hydroxymethyl-12-crown ether-4 on the surface of Li^+-IIP-Fe_3O_4@C was explored. Then, EGDMA (1 mL) and AIBN (2.5 mg) were added to the above mixture, the system was kept at 70 °C for 12 h. The obtained product was washed with 0.5 mol L^{-1} HNO_3 until no lithium ion was detected in the supernatant, and finally washed with distilled water until the pH was neutral and dried at 60 °C in oven. Thus, Li^+-IIP-Fe_3O_4@C prepared under the optimized conditions was obtained. The preparation process of Li^+-IIP-Fe_3O_4@C is shown in Fig. 1. For comparison, non-imprinted material (Li^+-NIP-Fe_3O_4@C) was also prepared under the same conditions without the addition of $LiClO_4$.

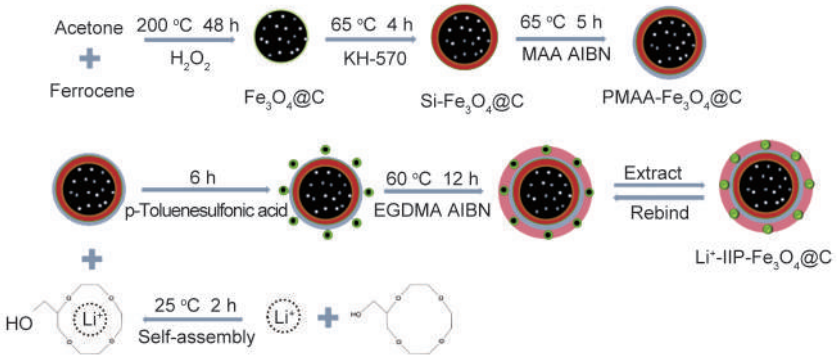

Fig. 1 The detailed illustration of preparation of Li^+-IIP-Fe_3O_4@C.

2.3 Characterization

The micromorphology of Fe_3O_4@C and Li^+-IIP-Fe_3O_4@C was characterized by using a JSM-6700F field scanning electron microscope (FESEM), Japan and a JEM-2100 high resolution transmission electron microscope (HRTEM), Japan. The composition of Fe_3O_4@C, Li^+-IIP-Fe_3O_4@C was analyzed by a Y2000 X-ray diffractometer (XRD), China. The surface functional groups of Fe_3O_4@C Si-Fe_3O_4@C, PMAA-Fe_3O_4@C, Li^+-IIP-Fe_3O_4@C were analyzed by a BRUKER FTS-165 Fourier transform infrared spectrometer (FTIR), Germany. The Setaram Labsys Evo thermogravimeter (TG), France was used for thermal analysis of Fe_3O_4@C, Si-Fe_3O_4@C, PMAA-Fe_3O_4@C, and Li^+-IIP-Fe_3O_4@C. Ion concentration in solutions was determined by a PerkinElmer Avio 200 inductively coupled plasma optical emission spectrometer (ICP-OES), USA.

2.4 Adsorption performance

2.4.1 Adsorption kinetics

Absorbent (5 mg) was added into the lithium solution (10 mL, 20 mg L^{-1}). The concentration of the solution after addition for 5, 10, 15, 20, 30, 60, 90 and 120 min was determined by an ICP-OES. The adsorption capacity of lithium was calculated by the following equation (2):

$$Q_t = (C_0 - C_t)V/m \quad (2)$$

Where Q_t (mg g^{-1}) represents the adsorption capacity at time t. C_0 (mg L^{-1}) and C_t (mg L^{-1}) are the initial concentration of lithium ion and the concentration of lithium ion at time t, respectively. V (L) is the volume of the solution, m (g) represents the mass of the lithium ion-imprinted adsorbent materials or non-imprinted adsorbent materials.

2.4.2 Isothermal adsorption

To determine the adsorption capacity of materials, the adsorption equilibrium experiment was performed. Absorbent (5 mg) was placed in 10 mL of solutions with different initial concentrations of Li^+ (10, 20, 40, 60, 100, 200, 300 mg L^{-1}) at 25 °C. After adsorption equilibrium, the concentration of Li^+ in the solution was measured by the ICP-OES. The equilibrium adsorption capacity of lithium ion-imprinted adsorbent material or non-imprinted adsorbent material was calculated as the following equation (3):

$$Q_e = (C_0 - C_e)V/m \quad (3)$$

Where Q_e (mg g^{-1}) represents equilibrium adsorption capacity and C_e (mg L^{-1}) is the equilibrium concentration of lithium ions.

2.4.3 Selective adsorption

Na^+, K^+ and Mg^{2+} were chosen as competitive ions to investigate the selectivity of materials. Adsorbent (5 mg) was put into 10 mL of a mixed solution containing 20 mg L^{-1} of Li^+, Na^+, K^+ and Mg^{2+}. After adsorption equilibrium, the concentrations of Li^+, Na^+, K^+ and Mg^{2+} in the solution were detected by the ICP-OES. The adsorption capacity of each ion by the lithium ion-imprinted adsorbent material or non-imprinted adsorbent material was calculated by the equation (4):

$$Q_M = (C_0 - C_e)V/m \quad (4)$$

where Q_M is the adsorption capacity of the material towards each ion.

2.4.4 Regeneration performance

The regeneration performance was studied by desorbing the adsorbed material with 0.5 mol L^{-1} HNO_3 solution to release lithium ions, and then the absorbent was used to absorb lithium ions again in 10 mL of 20 mg L^{-1} Li^+ solution. To test the regeneration performance of the lithium ion-mprinted material, adsorption-desorption was repeated for six times.

3 Results and discussion

3.1 Optimization of the initiator dosage during preparation of PMAA-Fe_3O_4@C

The grafting degree of MAA on the surface of PMAA-Fe_3O_4@C plays a crucial role in the immobilization of 2-hydroxymethyl-12-crown-4. And the initiator AIBN dosage directly affects the grafting efficiency of the functional monomer MAA. As shown in Fig. 2a-c, with increasing the AIBN dosage from 0.000 2 to 0.001 mol, PMAA-Fe_3O_4@C gradually agglomerates and exhibits irregular spherical morphology. The TG curve in Fig. 2d reflects the grafting efficiency of MAA on the surface of PMAA-Fe_3O_4@C. When the AIBN dosage increases from 0.000 2 to 0.000 5 mol, the grafting degree of MAA increases from 5.88% to 20.59%. As the initiator dosage further increases to 0.001 mol, the grafting degree of MAA increases to 26.47% but the product presents irregular and agglomerate morphology. Therefore, by taking MAA grafting degree and PMAA-Fe_3O_4@C morphology into consideration, the appropriate initiator dosage is 0.000 5 mol in this research.

3.2 Optimization of the catalyst dosage and reaction temperature during preparation of Li^+-IIP-Fe_3O_4@C

During the preparation of Li^+-IIP-Fe_3O_4@C, the catalyst (p-toluenesulfonic acid) dosage and reaction temperature play a key role in the immobilization of 2-hydroxymethyl-12-crown-4 on the surface of PMAA-Fe_3O_4@C, which influences the adsorption capacity of Li^+-IIP-Fe_3O_4@C. Therefore, the effects

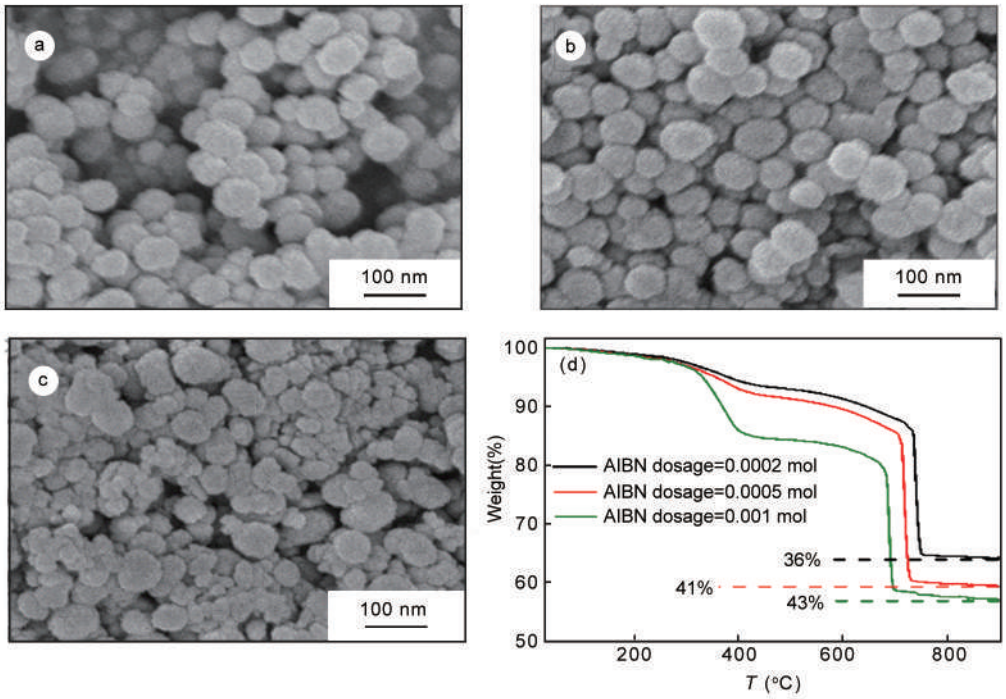

Fig. 2 SEM images at the initiator AIBN dosage of (a) 0.000 2 mol, (b) 0.000 5 mol, (c) 0.001 mol and (d) the corresponding TG curves of PMAA-Fe_3O_4@C.

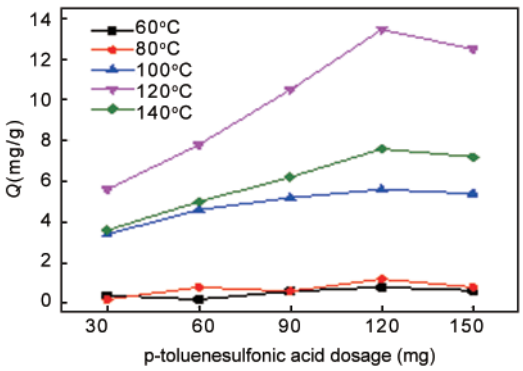

Fig. 3 Adsorption capacities of Li^+-IIP-Fe_3O_4@C prepared under different catalyst dosages at reaction temperatures from 60 to 140 °C.

of the p-toluenesulfonic acid dosage and reaction temperature on the Li^+ adsorption capacity of Li^+-IIP-Fe_3O_4@C are investigated, as shown in Fig. 3.

At lower reaction temperatures (60 and 80 °C), the obtained Li^+-IIP-Fe_3O_4@C has no obvious adsorption capacity towards Li^+. On the other hand, Li^+-IIP-Fe_3O_4@C shows hardly changing adsorption capacity towards Li^+ with increasing the p-toluenesulfonic acid dosage in the reaction system. This is because the reaction temperature is too low to activate 2-hydroxymethyl-12-crown-4. Therefore, these conditions are unfavorable for the immobilization of 2-hydroxymethyl-12-crown-4 on the surface of PMAA-Fe_3O_4@C, which affects the Li^+ adsorption capacity of Li^+-IIP-Fe_3O_4@C, resulting in negligible adsorption capacity. When the reaction temperature increases to 100 °C, the resultant Li^+-IIP-Fe_3O_4@C shows a much improved adsorption capacity for Li^+, indicating that 2-hydroxymethyl-12-crown-4 is grafted and immobilized on PMAAFe_3O_4@C under catalysis of p-toluenesulfonic acid under 100 °C, which improves the adsorption capacity of Li^+-IIP-Fe_3O_4@C towards Li^+ significantly. When the reaction temperature increases to 120 °C, Li^+-IIP-Fe_3O_4@C prepared with the p-toluenesulfonic acid dosage of 120 mg exhibits the maximum adsorption capacity. This shows that at a high reaction temperature of 120 °C, 2-hydroxymethyl-12-crown-4 molecules are activated, and then immobilized onto the surface of PMAA-Fe_3O_4@C under catalysis of p-toluenesulfonic acid. Therefore, the adsorption capacity of Li^+ is further improved, resulting in an improved adsorption capacity of Li^+-IIP-Fe_3O_4@C. As the reaction temperature increases further to 140 °C, which approaches the boiling point of 2-hydroxymethyl-12-crown-4, 2-hydroxymethyl-12-crown-4 molecules are vaporized, which decreases their immobilization efficiency onto the surface of PMAA-Fe_3O_4@C, and finally reduces the adsorption capacity for Li^+. Therefore, by comparing the adsorption capacity of Li^+-IIP-Fe_3O_4@C prepared under different conditions, the optimal reaction temperature is 120 °C, and catalyst dosage is 120 mg. Thus, the structure

and properties of Li^+-IIP-Fe_3O_4@C prepared under the optimized conditions are analyzed in the subsequent sections.

3.3 Microstructure and magnetic properties

The morphology of Fe_3O_4@C and Li^+-IIP-Fe_3O_4@C was obtained by FESEM, as shown in Fig. 4. As shown in Fig. 4a-b, Fe_3O_4@C is spherical with a regular shape and uniform particle size. Li^+-IIP-Fe_3O_4@C, which was prepared by using Fe_3O_4@C as the matrix carrier, still maintains spherical morphology, but the particle size of Li^+-IIP-Fe_3O_4@C increases due to the graft polymerization of the adsorption unit 2-hydroxymethyl-12-crown-4 and cross-linking agent EGDMA in the imprinting process. Further, HRTEM was used to characterize the microstructure of Li^+-IIP-Fe_3O_4@C. It can be seen from Fig. 4c-d that Li^+-IIP-Fe_3O_4@C possesses a core-shell structure and the inner core is Fe_3O_4@C nanoparticle.

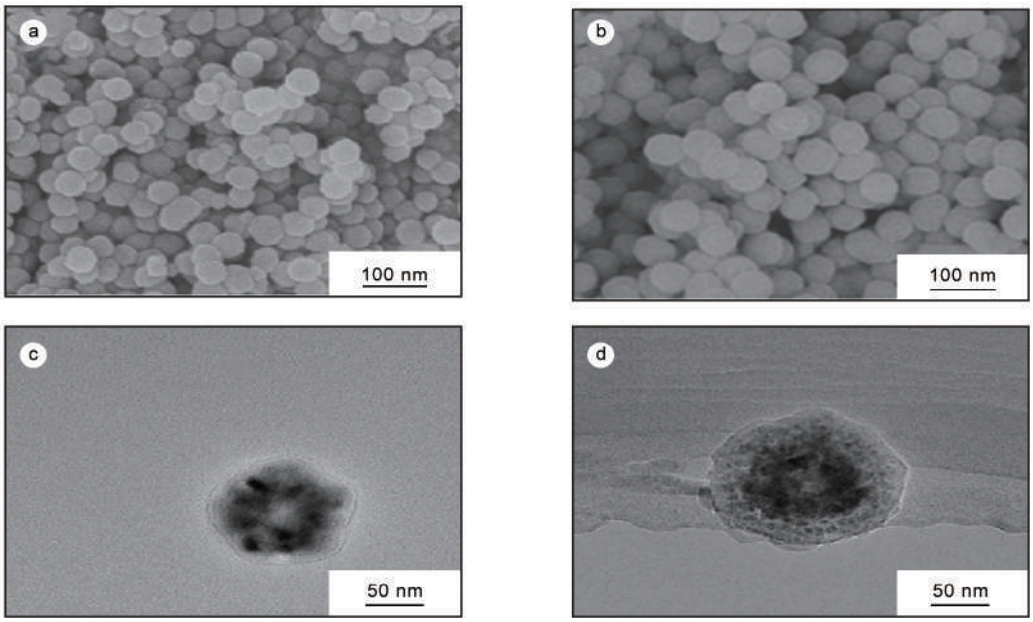

Fig. 4　FESEM images of (a) Fe_3O_4@C and (b) Li^+-IIP-Fe_3O_4@C, and HRTEM images of (c) Fe_3O_4@C and (d) Li^+-IIP-Fe_3O_4@C.

By analysis of FT-IR spectra (Fig. 5a), the surface functional groups at each modification stage can be identified. The band at 590 cm^{-1} in Fe_3O_4@C is attributed to the stretching vibration of Fe-O-Fe of Fe_3O_4 particles. The adsorption band at 1 050 cm^{-1} of Si-Fe_3O_4@C corresponds to the tensile vibration of C—O—Si, which is due to the silanization of KH-570. The absorption of C—H at 2 974 cm^{-1} is caused by the grafting of MAA. The unique absorption band of Li^+-IIP-Fe_3O_4@C at 1 278 cm^{-1} is due to C—O—C stretching vibration, which proves the presence of 2-hydroxymethyl-12-crown-4 on the surface of carbon nanospheres. The appearance of characteristic functional groups of the products at each stage not only indicates the realization of modification at each stage, but also provides the possibility of constructing lithium-imprinted sites.

To confirm the thermostability of the products in each reaction stage, the TG test was performed in Ar atmosphere at the temperature range from 0 to 900 °C at a heating rate of 10 °C min^{-1}, as shown in Fig. 5b. It can be seen that the weight loss of the products in each stage gradually increases in the temperature range up to 600 °C, suggesting a high stability. For Fe_3O_4@C, its weight loss is 7% at 600 °C, while that of Si-Fe_3O_4@C is 8%, only 1% higher. This is due to the fact that thermal decomposition of KH-i570 leads to the formation of silicon oxide, which hinders the further decomposition of Si-Fe_3O_4@C. After grafting MAA, PMAA-Fe_3O_4@C shows a suddenly increased weight loss of 11%, due to the large amount of MAA grafted onto its surface. Compared with PMAA-Fe_3O_4@C, Li^+-IIP-Fe_3O_4@C increases in weight loss by 2% after cross-linking polymerization. When the temperature is raised from 600 to 700 °C, the weight loss of all the products in each stage shows an abrupt increase, which is caused by the carbothermal reduction between carbon and Fe_3O_4. Within the temperature range of 700-900 °C, the thermogravimetric curves of the products in each stage are flattened because of the completion of carbothermal reduction.

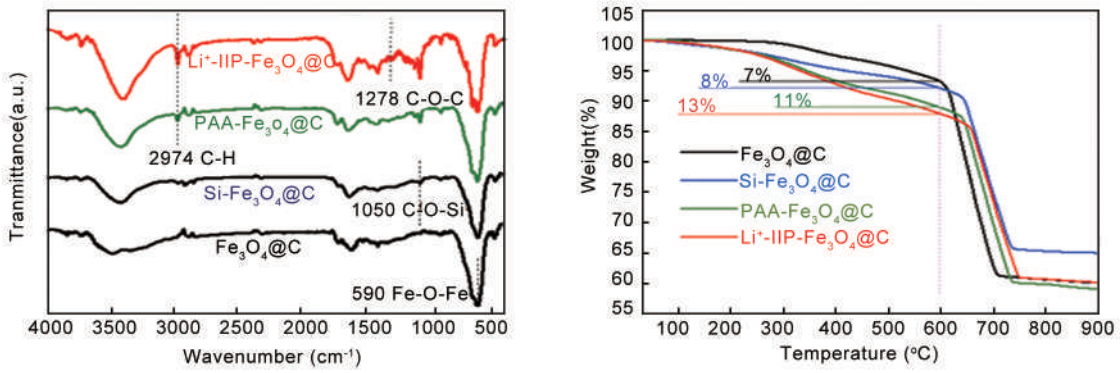

Fig. 5 (a) FT-IR spectra and (b) TG diagram in Ar of each stage product at a heating rate of 10 °C/min.

The magnetic response property of Li^+-IIP-Fe_3O_4@C is conferred by Fe_3O_4 particles. In Fig. 6, XRD analysis was performed onFe_3O_4@C and Li^+-IIP-Fe_3O_4@C, and the results are compared with the characteristic peaks of Fe_3O_4 in the PDF card. From Fig. 6, it can be seen that both Fe_3O_4@C and Li^+-IIP-Fe_3O_4@C have peaks of (220), (311), (400), (422), (511) and (440) at 2 angles of 30°, 36°, 43°, 53°, 57°, 63°, respectively, which are ascribed to the diffraction peaks of Fe_3O_4. These results show that Li^+-IIP-Fe_3O_4@C has a cubic structure of Fe_3O_4, which provides the possibility of subsequent liquid solid separation and recycling.

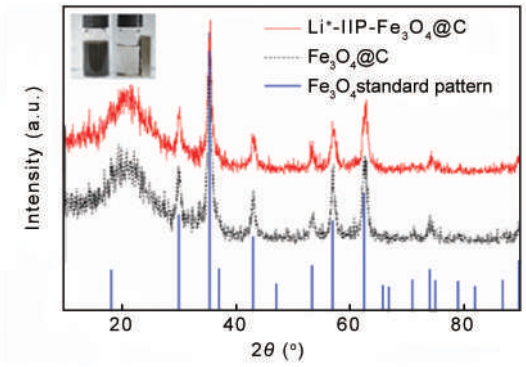

Fig. 6 XRD of Fe_3O_4@C and Li^+-IIP-Fe_3O_4@C (inset image: magnetic separation of Li^+-IIP-Fe_3O_4@C in water).

According to the previous research, the saturation magnetization of Fe_3O_4@C is 32.2 emu g^{-1}, suggesting Fe_3O_4@C could be easily separated from solution by applying an external magnetic field[31]. As shown in the inset image in Fig. 6, Li^+-IIP-Fe_3O_4@C synthesized with Fe_3O_4@C as a carrier, can be easy to achieve solid-liquid separation under an external magnetic field because of its good magnetic properties of Fe_3O_4@C.

3.4 Adsorption performance

3.4.1 Adsorption kinetics

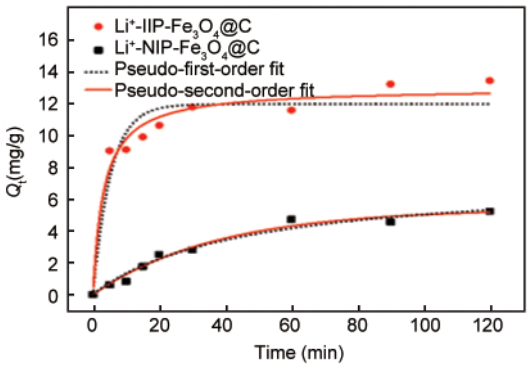

Fig. 7 Adsorption kinetics curves of Li^+-IIP-Fe_3O_4@C and Li^+-NIP-Fe_3O_4@C.

The adsorption kinetic curves of Li^+-IIP-Fe_3O_4@C and Li^+-NIP-Fe_3O_4@C are shown in Fig. 7. Both Li^+-IIP-Fe_3O_4@C and Li^+-IIP-Fe_3O_4@C show adsorption towards lithium ions. As time goes by, the adsorption capacity of the two materials towards lithium ions increases rapidly in the first 30 min, and then levels off with the increase of time. The imprinted cavities and binding sites on the material surface are abundant at the initial stage of adsorption, thus Li^+ can be quickly identified and adsorbed. As the adsorption continues, the adsorption rate gradually decreases as most of the recognition sites are occupied. When the adsorption time is extended to 120 min, both absorbents reach the adsorption equilibrium. Moreover, the adsorption capacities of Li^+-IIP-Fe_3O_4@C in different time periods are always higher than those of Li^+-IIP-Fe_3O_4@C, which indicates that Li^+-IIP-Fe_3O_4@C has the specific recognition sites towards the template ions.

To reveal the mechanism behind lithium ion adsorption kinetics, the pseudo-first-order and second-order kinetic models were fitted to the adsorption kinetic data by the equations (5) and (6) respectively[33]. The fitting results are shown in Table 1.

$$Q_t = Q_e - Q_e e^{-k_1 t} \quad (5)$$

$$Q_t = k_2 Q_e^2 t/(1 + k_2 Q_t t) \quad (6)$$

Where Q_e (mg g^{-1}) is the equilibrium adsorption capacity of lithium. Q_t (mg g^{-1}) is the amount of adsorption at time t. k_1 (1 min^{-1}) and k_2 (g (mg min)$^{-1}$) are constants of the first-order and second-order kinetic models, respectively.

Table 1 shows the kinetic adsorption parameters of Li^+-IIP-Fe_3O_4@C and Li^+-NIP-Fe_3O_4@C. The R^2 of the pseudo-second-order kinetic model (0.966 4) is higher than that of the pseudo-first-order dynamic model (0.915 8). As shown in Table 1, the calculated adsorption capacity ($Q_{e,\ cal}$ = 12.99 mg g^{-1}) for the pseudo-second-order kinetic model is close to the experimental value ($Q_{e,\ exp}$ = 13.46 mg g^{-1}). These findings indicate that it is more appropriate to describe the adsorption behavior of Li^+-IIP-Fe_3O_4@C towards lithium ions with the pseudo-second-order kinetic model, suggesting that the chemical adsorption nature of lithium ions by Li^+-IIP-Fe_3O_4@C due to the complex interactions between multiple C-Os of crown ether and lithium ions.

Table 1　Kinetic adsorption parameters of Li^+-IIP-Fe_3O_4@C and Li^+-NIP-Fe_3O_4@C.

Kinetic models		Pseudo-first-order-model			Pseudo-second-order-model		
Absorbents	$Q_{e,\ exp}$	$Q_{e,\ cal}$	k_1	R^2	$Q_{e,\ cal}$	k_2	R^2
Li^+-IIP-Fe_3O_4@C	13.46	11.98	0.1896	0.9158	12.99	0.0236	0.9664
Li^+-NIP-Fe_3O_4@C	5.24	7.34	0.0030	0.9744	5.40	0.0266	0.9796

Note: $Q_{e,\ exp}$ is the experimental value of Q_e (mg g^{-1}); $Q_{e,\ cal}$ is the calculated value of Q_e (mg g^{-1}).

3.4.2　Adsorption isotherms

It can be seen from the adsorption isotherms of Li^+-IIP-Fe_3O_4@C and Li^+-NIP-Fe_3O_4@C in Fig. 8 that the adsorption capacities of two absorbents increase with the increase of the lithium ion concentration. As the lithium ion concentration increases to 100 mg L^{-1}, the adsorption is basically saturated. Then as the concentration continues to increase to 300 mg L^{-1}, there is no significant change in the adsorption capacity. The maximum adsorption capacity of Li^+-IIP-Fe_3O_4@C (22.26 mg g^{-1}) is higher than that of Li^+-NIP-Fe_3O_4@C (11.94 mg g^{-1}). And the imprinting factor (f_{imp}), which is calculated by the equation (7), is 1.86.

$$f_{imp} = Q_{e(IIP)}/Q_{e(NIP)} \quad (7)$$

Where $Q_{e(IIP)}$ and $Q_{e(NIP)}$ represent the equilibrium adsorption capacity of Li^+-IIP-Fe_3O_4 @ C and Li^+-NIP-Fe_3O_4 @ C, respectively. These findings prove that Li^+-IIP-Fe_3O_4@C has an excellent adsorption selectivity towards Li^+.

The experimental data are fitted to the Langmuir and Freundlich isotherm models using the equations (8) and (9), respectively. The fitting results are shown in Table 2. It can be seen from Table 2 that the correlation coefficient of the Langmuir isotherm model (0.958 5) is significantly better than that of the Freundlich isotherm model (0.905 9). In addition, the adsorption capacity calculated by the Langmuir isotherm model is close to the experimental results. These results suggest that the adsorption for Li^+ can be described by monolayer adsorption. This adsorption behavior matches the imprinted layer constructed on the surface of carbon nanospheres by surface ion imprinting. Lithium ions can be captured by direct contact with the surface imprinting layer.

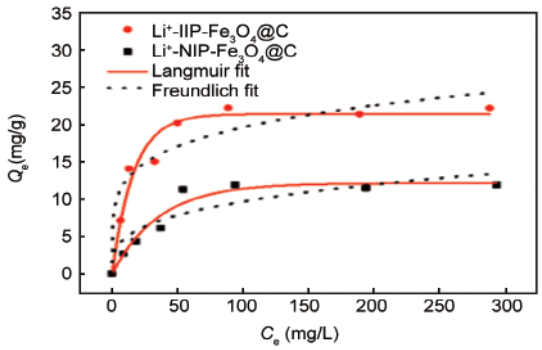

Fig. 8　Adsorption isotherm fitting curves of Li^+-IIP-Fe_3O_4@C and Li^+-NIP-Fe_3O_4@C.

$$Q_e = K_L Q_m C_e/(1 + K_L C_e) \quad (8)$$

$$Q_e = K_F C_e^{1/n} \quad (9)$$

Where Q_m (mg g^{-1}) is the maximum adsorption capacity of material, K_L (L mg^{-1}) is the Langmuir constant, and K_F (mg L^{-1}) and $1/n$ are Freundlich constants.

The binding affinity of an adsorbent towards a target ion is analyzed according to the separation factor R_L value calculated by the equation (10) according to the K_L constant in the Langmuir isotherm model. The value of R_L is between 0 and 1. The smaller the value of R_L is, the more favorable it is for the adsorbent to adsorb the target ion. The R_L value of Li^+-IIP-Fe_3O_4@C is calculated to be 0.051 9, which proves that lithium ions are easily adsorbed by this material due to the strong binding affinity between the absorbent and target ions.

$$R_L = 1/(1 + C_m K_L) \quad (10)$$

Where C_m (mg L^{-1}) is the maximum initial concentration and K_L ($L\ mg^{-1}$) is Langmuir constant.

Table 2 Isothermal adsorption parameters of Li^+-IIP-Fe_3O_4@C and Li^+-NIP-Fe_3O_4@C.

Isothermal models		Langmuir model			Freundlich model		
Absorbents	$Q_{e,exp}$	$Q_{e,cal}$	K_L	R^2	K_F	$1/n$	R^2
Li^+-IIP-Fe_3O_4@C	22.26	21.43	0.0609	0.9585	7.7935	0.2007	0.9059
Li^+-NIP-Fe_3O_4@C	11.94	12.16	0.0278	0.9552	2.3889	0.3043	0.8416

Note: $Q_{e,exp}$ is the experimental value of Q_e (mg g^{-1}), $Q_{e,cal}$ is the calculated value of Q_e (mg g^{-1}) of the Langmuir adsorption model.

Table 3 Adsorption selectivity of Li^+-IIP-Fe_3O_4@C for Li^+.

Ions	Li^+-IIP-Fe_3O_4@C		Li^+-NIP-Fe_3O_4@C		α'
	K_d	α_M^{Li+}	K_d	α_M^{Li+}	
Li^+	1.03	-	0.25	-	-
Na^+	0.13	8.06	0.10	2.67	3.02
K^+	0.18	5.72	0.13	2.00	2.86
Mg^{2+}	0.37	2.75	0.12	2.06	1.31

Table 4 Comparison with other adsorbents for Li^+ adsorption performance.

Absorbents	Adsorption capacity (mg g^{-1})	Selective factor (α_{Na}^{Li+}, α_K^{Li+})	Regeneration performance	Reference
Li-IIPs	6.79	5.34, 6.47	95% (six cycles)	[25]
Fe_3O_4@SiO_2@IIP	4.07	50.88, 42.38	92% (five cycles)	[26]
LIPs	9.46	3.66, 3.01	89.7% (ten cycles)	[27]
DIMFs	26.2	72.05, 93.35	85% (five cycles)	[33]
Li^+-IIP	7.07	24.15, 52.1	97.9% (five cycles)	[34]
Li^+-IIP-Fe_3O_4@C	22.94	8.06, 5.72	91.2% (six cycles)	This work

3.4.3 Selective adsorption

To investigate the adsorption selectivity of Li^+-IIP-Fe_3O_4@C towards Li^+ against other metal ions with similar or large size, Na^+ (0.204 nm), K^+ (0.276 nm) and Mg^{2+} (0.144 nm) were selected as the competitive ions. The adsorption capacities of Li^+-IIP-Fe_3O_4@C for the four ions are shown in Fig. 9. Compared with the adsorption capacities for Na^+ (1.66 mg g^{-1}), K^+ (2.34 mg g^{-1}), Mg^{2+} (3.36 mg g^{-1}), a significantly higher adsorption capacity for Li^+ (12.72 mg g^{-1}) is observed. This is because the formed imprinted cavities have a closer size to and thus stronger electrostatic interaction with the target ion than to other ions.

The distribution coefficient K_d, selection factor $\alpha_M^{Li^+}$ and relative selection factor of Li^+-IIP-Fe_3O_4@C towards Li^+ against the other three competitive ions can be calculated by the equations (11), (12) and (13). The results are shown in Table 3.

$$K_d = (C_0 - C_e)V/(C_e m) \quad (11)$$

$$\alpha_M^{Li^+} = K_d^{Li}/K_d^{M} (M = Na^+, K^+, Mg^{2+}) \quad (12)$$

$$\alpha' = \alpha_x^{Li^+}(I)/\alpha_x^{Li^+}(N) \quad (13)$$

Where C_0 (mg L^{-1}) and C_e (mg L^{-1}) represent the initial concentration and equilibrium concentration of ions, Q_M (mg g^{-1}) is the adsorption capacity of material to each ion, V (L) is the volume of the solution, and m (g) is the mass of lithium ion-imprinted adsorbent or non-imprinted adsorbent.

Obviously, the K_d value of Li^+-IIP-Fe_3O_4@C for Li^+ (1.03) is greater than that for Na^+ (0.13), K^+ (0.18), and Mg^{2+} (0.37). This is consistent with the results exhibited by the selection factor, indicating that Li^+-IIP-Fe_3O_4@C has a higher separation selectivity towards Li^+. Further, according to the α' values, Li^+-IIP-Fe_3O_4@C has a higher selective recognition towards Li^+ than Li^+-NIP-Fe_3O_4@C.

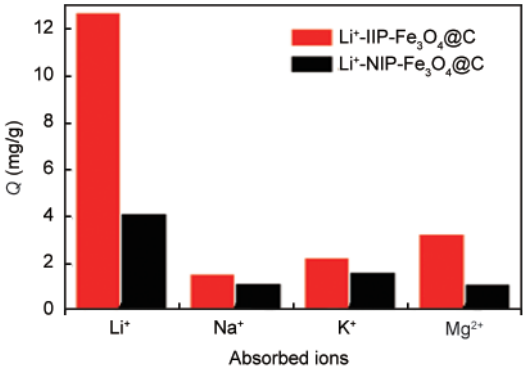

Fig. 9 Adsorption selectivity of Li^+-IIP-Fe_3O_4@C.

3.4.4 Regeneration performance

The adsorption-desorption cycle is used to investigate whether the material has good regeneration performance. Fig. 10 shows the adsorption capacity of Li^+-IIP-Fe_3O_4@C after six adsorption-desorption cycles. It can be seen that the adsorption capacity of Li^+-IIP-Fe_3O_4@C towards Li^+ decreases slightly from 13.84 to 12.62 mg g^{-1} after six adsorption-desorption cycles, only a 8.8% decrease. This slight

decrease is due to the damage of the adsorption sites using HNO_3 as an eluent during desorption. Despite this, Li^+-IIP-Fe_3O_4@C still shows good regeneration performance with high recovery rates ranging from 97.27% to 96.12% in six adsorption-desorption cycles.

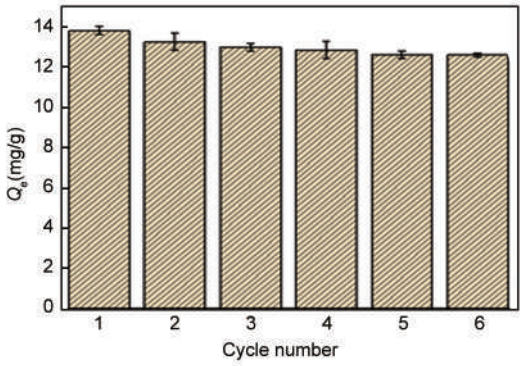

Fig. 10　Li^+-IIP-Fe_3O_4@C adsorption and regeneration performance of Li^+.

As shown in Table 4, the adsorption of different materials for Li^+ are compared. It can be seen that the Li^+-IIP-Fe_3O_4@C in this work has a considerable adsorption capacity for Li^+. Importantly, it also has a better selectivity and regeneration performance for extracting Li^+. Therefore, the Li^+-IIP-Fe_3O_4@C in this work can be regard as a kind of potential material for selectively extracting Li^+ with a high recycling utilization rate.

4　Conclusions

PMAA-Fe_3O_4@C, with uniform morphology and a high MAA grafting efficiency of 20.59%, was synthesized under a molar ratio of AIBN to MAA of 1∶20. On this basis, Li^+-IIP-Fe_3O_4@C with a high selectivity for Li^+ adsorption was synthesized under a molar ratio of 2-hydroxymethyl-12-crown-4 to p-toluenesulfonic acid of 1∶1.39 at 120 °C. Li^+-IIP-Fe_3O_4@C achieves a high selectivity factor for Li^+ relative to Na^+ (8.06), K^+ (5.72), Mg^{2+} (2.75) in a solution with a lithium ion concentration of 20 mg L^{-1} for each at 25 °C. The maximum adsorption capacity of Li^+-Fe_3O_4@C (22.26 mg g^{-1}) is 1.86 times that of non-imprinted material (11.94 mg g^{-1}). The adsorption of Li^+-IIP-Fe_3O_4@C is better described by the Langmuir isotherm model and the pseudo-second-order kinetic model. More importantly, after adsorption-desorption cycles, the recognition ability only decreases by 8.8% of the initial value, suggesting that the prepared Li^+-IIP-Fe_3O_4@C has excellent regeneration performance and a high stability. The ion-imprinted product is expected to be used for separation and recovery of lithium ions from the salt lake water.

References

[1] Martin G, Rentsch L, Höck M, et al. Lithium market research-global supply, future demand and price development[J]. Energy Storage Materials, 2017, 6: 171-179.

[2] Swain B. Recovery and recycling of lithium: A review[J]. Separation and Purification Technology, 2017, 172: 388-403.

[3] Xiang W, Liang S K, Zhou Z Y, et al. Extraction of lithium from salt lake brine containing borate anion and high concentration of magnesium[J]. Hydrometallurgy, 2016, 166: 9-15.

[4] Liu D H, Gao X Y, An H Z, et al. Supply and demand response trends of lithium resources driven by the demand of emerging renewable energy technologies in China[J]. Resources, Conservation and Recycling, 2019, 145: 311-321.

[5] Song J F, Nghiem L D, Li X M, et al. Lithium extraction from Chinese salt-lake brines: Opportunities, challenges, and future outlook[J]. Environmental Science: Water Research & Technology, 2017, 3: 593-597.

[6] Wang S L, Zheng S L, Wang Z M, et al. Superior lithium adsorption and required magnetic separation behavior of iron-doped lithium ion – sieves[J]. Chemical Engineering Journal, 2018, 332: 160-168.

[7] Özgür C. Preparation and characterization of $LiMn_2O_4$ ion-sieve with high Li^+ adsorption rate by ultrasonic spray pyrolysis[J]. Solid State Ionics 2010, 181: 1425-1428.

[8] Wang L, Ma W, Liu R, et al. Correlation between Li^+ adsorption capacity and the preparation conditions of spinel lithium manganese precursor[J]. Solid State Ionics 2006, 177: 1421-1428.

[9] Zhang L C, Li L J, Shi D, et al. Recovery of lithium from alkaline brine by solvent extraction with β-diketone[J]. Hydrometallurgy 2018, 175: 35-42.

[10] Gao D L, Yu X P, Guo Y F, et al. Extraction of lithium from salt lake brine with triisobutyl phosphate in ionic liquid and kerosene[J]. Chemical Research in Chinese Universities, 2015, 31: 621-626.

[11] Chen P, Tang S Y, Yue H R, et al. Lithium enrichment of high Mg/Li ratio brine by precipitation of magnesium via combined CO_2 mineralization and solvent extraction[J]. Industrial & Engineering Chemistry Research, 2017, 56: 5668-5678.

[12] Zheng M P, Zhang Y S, Liu X F, et al. Progress and prospects of salt lake research in China[J]. Acta Geologica Sinica-English Edition, 2016, 90: 1195-1235.

[13] Huang W, Liu S C, Liu J X, et al. 2-Methylol-12-crown-4 ether immobilized PolyHIPEs toward recovery of lithium (I)[J]. New Journal of Chemistry, 2018, 42: 16814-16822.

[14] Xu J C, Pu Z L, Xu X C, et al. Simultaneous adsorption of Li (I) and Rb (I) by dual crown ethers modified magnetic ion imprinting polymers[J]. Applied Organometallic Chemistry, 2019, 33: e4778.

[15] Yang Y Z, Liu X G, Xu B S. Recent advances in molecular imprinting technology for the deep desulfurization of fuel oils[J]. New Carbon Materials, 2014, 29(1): 1-14.

[16] Zhao X F, Duan F F, Cui P P, et al. A molecularly-imprinted polymer decorated on graphene oxide for the selective recogni-

tion of quercetin[J]. New Carbon Materials, 2018, 33(6): 529-543.

[17] Saloni J, Walker K, Glake H, et al. Theoretical investigation on monomer and solvent selection for molecular imprinting of nitrocompounds[J]. The Journal of Physical Chemistry A, 2013, 117: 1531-1534.

[18] Zhai Y H, Liu Y W, Chang X J, et al. Selective solid-phase extraction of trace cadmium (II) with an ionic imprinted polymer prepared from a dual-ligand monomer[J]. Analytica Chimica Acta, 2007, 593: 123-128.

[19] Diao K S, Wang H J, Qiu Z M, A DFT study on the selective extraction of metallic ions by 12-crown-4[J]. Journal of Solution Chemistry, 2009, 38: 713-724.

[20] Mehrdad Y, Mir M Z, Morteza Z. Lithium removal from seawater via liquid membrane transport using 12-crown-4 as a carrier and study of the effect of carbon nanotubes as a membrane additive[J]. Analytical Methods, 2019, 11: 2720-2725.

[21] Sun D S, Zhu Y Z, Meng M J, et al. Fabrication of highly selective ion imprinted macroporous membranes with crown ether for targeted separation of lithium ion[J]. Separation and Purification Technology, 2017, 175: 19-26.

[22] Swain B. Separation and purification of lithium by solvent extraction and supported liquid membrane, analysis of their mechanism: a review[J]. Journal of Chemical Technology & Biotechnology, 2016, 91: 2549-2562.

[23] Calvo Muñoz E M, García Mateos F J, Rosas J M, et al. Biomass waste carbon materials as adsorbents for CO_2 capture under post-combustion conditions[J]. Frontiers in Materials, 2016, 3: 23.

[24] Beralus J M, Ruiz Rosas R, Cazorla Amorós D, et al. Electroadsorption of arsenic from natural water in granular activated carbon[J]. Frontiers in Materials, 2014, 1: 28.

[25] Cui J Y, Zhou Z P, Liu S J, et al. Synthesis of cauliflower-like ion imprinted polymers for selective adsorption and separation of lithium ion[J]. New Journal of Chemistry, 2018, 42: 14502-14509.

[26] Luo X B, Guo B, Luo J M, et al. Recovery of lithium from wastewater using development of Li ion-imprinted polymers [J]. ACS Sustainable Chemistry & Engineering, 2015, 3: 460-467.

[27] Huang Y, Wang R. An efficient lithium ion imprinted adsorbent using multi-wall carbon nanotubes as support to recover lithium from water[J]. Journal of Cleaner Production, 2018, 205: 201-209.

[28] Wang J, Zhang W H, Qian Y C, et al. pH, temperature, and magnetic triple-responsive polymer porous microspheres for tunable adsorption[J]. Macromolecular Materials and Engineering, 2016, 301: 1132-1141.

[29] Yang Y Z, Song J J, Han Y X, et al. Self assembly of SiO_2-encapsulated carbon microsphere composites[J]. Applied Surface Science, 2011, 257: 7326-7329.

[30] Xue B X, Niu M, Yang Y Z, et al. Multi-functional carbon microspheres with double shell layers for flame retardant poly (ethylene terephthalate)[J]. Applied Surface Science, 2018, 435: 656-665.

[31] Shi W P, Liu W F, Chen L, et al. Effect of annealing temperature on the structure of carbon encapsulated Fe_3O_4 nanospheres [J]. RSC Advances, 2015, 5: 106787-106794.

[32] Liu W F, Qin L, An Z L, et al. Thermo-responsive ion imprinted polymer on the surface of magnetic carbon microspheres for identification and removal of low-concentrations of Cu^{2+} [J]. Environmental Chemistry, 2018, 15: 306-316.

[33] Wang Y Y, Xu J C, Yang D Y, et al. Calix [4] arenes functionalized dual-imprinted mesoporous film for the simultaneous selective recovery of lithium and rubidium[J]. Applied Organometallic Chemistry, 2018, 32: e4511.

[34] Hashemi B, Shamsipur M, Seyedzadeh Z. Synthesis of ion imprinted polymeric nanoparticles for selective pre-concentration and recognition of lithium ions[J]. New Journal of Chemistry, 2016, 40: 4803-4809.